DOI: 10.1002/chem.200700155

Electron-Transfer Reactions through the Associated Interaction between Cytochrome *c* and Self-Assembled Monolayers of Optically Active Cobalt(III) Complexes: Molecular Recognition Ability Induced by the Chirality of the Cobalt(III) Units

Isao Takahashi, Tomohiko Inomata, Yasuhiro Funahashi, Tomohiro Ozawa, and Hideki Masuda*[a]

Abstract: Self-assembled monolayers (SAMs) of optically active Co^{III} complexes ((*S*)-**2**/(*R*)-**2**) that contain (*S*)- or (*R*)-phenylalanine derivatives as a molecular recognition site were constructed on Au electrodes ((*S*)-**2**–Au/(*R*)-**2**–Au). Molecular recognition characteristics induced by the *S* and *R* configurations were investigated by measurements of electron-transfer reactions with horse heart cytochrome *c* (cyt *c*). The electrochemical studies indicate that the maximum current of cyt *c* reduction is obtained when the Au electrode is modified by **2** with a moderate coverage of approximately 4.0×10^{-11} mol cm^{-2}. Since the Au electrode is not densely packed with the Co^{III} units at this concentration, we conclude that the penetrative association process between cyt *c* and the Co^{III} unit plays an important role in this electron-transfer system. The differences in the electron-transfer rates of (*S*)-**2**–Au and (*R*)-**2**–Au increase with increasing scan rates, a result indicating that the chiral ligand has an influence on the rate of association of the complexes with cyt *c*. **3**–Au has a mixed monolayer composed of **2** and hexanethiol and exhibits electron-transfer behavior comparable to **2**–Au. The difference in the association rates of (*S*)-**3**–Au and (*R*)-**3**–Au is larger than that between (*S*)-**2**–Au and (*R*)-**2**–Au, which indicates that the molecular recognition ability of **3**–Au has been enhanced by filling the gap between molecules of **2** with hexanethiols. The differences in the oxidation rates of cyt c^{II} between (*S*)-**2**–Au and (*R*)-**2**–Au and between (*S*)-**3**–Au and (*R*)-**3**–Au were larger than the differences in the rates of the reduction of cyt c^{III}; this suggests that the size of the heme crevice varies according to the oxidation state of cyt *c*.

Keywords: chirality · cobalt · cytochrome *c* · electron transfer · molecular recognition

Introduction

Electron-transfer proteins such as cytochromes and azurins play a central role in biological electron-transport systems that contribute to photosynthesis and respiration.[1,2] Electron-transport systems depend upon the processes of accepting and donating electrons and on the process of recognition of redox partners. In a number of studies, horse heart cytochrome *c* (cyt *c*), a well-characterized respiratory electron-transport protein, has been used as a probe for investigation of the biological functions of other electron-transport proteins.[3–14] Cyt *c* accepts electrons from cytochrome *c* reductase and donates electrons to cytochrome *c* peroxidase and cytochrome *c* oxidase at the end of the respiratory electron–transport chain.[3] Investigations with various lysine-modified versions of cyt *c* have concluded that the intermolecular electron-transfer reactions are facilitated by interaction of the positively charged cyt *c* with the negatively charged surfaces of its redox partners.[4–9] The intermolecular van der Waals, hydrogen bonding, and electrostatic interactions involved in the formation of the associated complexes of cyt *c* with cytochrome *c* reductase or with cytochrome *c* peroxidase have been characterized from crystal structures of these complexes.[13,14] These noncovalent interactions occur at multiple sites within the associated complexes. Unfortunately, it is quite difficult to explore noncovalent interac-

[a] Dr. I. Takahashi, Dr. T. Inomata, Dr. Y. Funahashi, Dr. T. Ozawa, Prof. Dr. H. Masuda
Department of Applied Chemistry
Nagoya Institute of Technology
Showa-ku, Nagoya 466-8555 (Japan)
Fax: (+81) 52-735-5209
E-mail: masuda.hideki@nitech.ac.jp

Supporting information for this article is available on the WWW under http://www.chemeurj.org/ or from the author.

tions other than electrostatic interactions by using current methodologies.

As the redox-active heme iron atom of cyt *c* is buried within the interior of the protein,[15] the redox wave of cyt *c* cannot be observed by using rare-metal electrodes such as Au, Ag, and Pt. In 1977, Hill and co-workers first reported the reversible redox behavior of cyt *c* by using a system comprising self-assembled monolayers (SAMs) of 4,4′-bipyridine.[16a] Subsequently, the electrochemical properties of cyt *c* were examined by using SAMs with various bifunctional molecules that include sites for adsorption to electrode surfaces as well as sites for interaction with cyt *c*.[16–31] The modified molecules are defined as "promoters" of heterogeneous electron-transfer reactions between cyt *c* and an electrode surface, despite the fact that they are redox inactive within the redox range of cyt *c*. Over 50 different promoters for cyt *c* have been reported[16–22] since the first report of Hill and co-workers.[16a] Taniguchi et al. have demonstrated the importance of hydrogen-bonding interactions between the lysine residues of cyt *c* and the nitrogen atoms of the pyridine on an Au surface by using mercaptopyridine.[18] The SAM of the negatively charged complex $[Ru^{II}(CN)_5(4\text{-pyS})]^{4-}$ (4-pyS: 4-mercaptopyridine) also produced a reversible redox wave with cyt *c*.[20] Therefore, the promoting ability is strongly affected by noncovalent interactions between promoters and the lysine residues of cyt *c*. Promoter capability requires interaction with the positively charged cyt *c* surface, but it does not require local interactions with the recognition site of cyt *c*. As yet, there have been no attempts to produce a promoter capable of interacting directly with the cyt *c* recognition site as this would necessitate the design of a patterned indented surface for investigating the recognition between cyt *c* and the promoter itself.

Waldeck and co-workers have reported direct-wiring systems based on a mixed monolayer of *n*-alkanethiols and pyridine-terminated alkanethiols coordinating to the heme Fe atom of cyt *c*.[31] This system exhibited clear redox waves, in contrast to examples with single monolayers of pyridine-terminated alkanethiols. Whitesides and co-workers used surface plasmon resonance measurements to investigate the association/dissociation process of carbonic anhydrase (CA) on an arylsulfonamide (ASA) modified Au surface through coordination of the Zn center of CA.[32,33] In the case of a mixed monolayer of ASA and tri(ethylene glycol) derivatives, the binding of CA occurred through reversible linkage to the surface of the ASA units when the surface density of the ASA units was very low, while the adsorption rate of CA drastically decreased with an increasing surface density of ASA units. This led to the proposal that this decrease in rate was due to steric repulsion between CA molecules.

As these previously investigated systems have proteins immobilized through coordination to metal centers, the structures of the immobilized proteins would not be expected to retain their native forms, because of alteration of the local structure around the metal centers.

We previously investigated SAMs of optically active Co^{III} complex **2** by probing the structural environment at the electron-transfer site of native cyt *c* (Scheme 1).[34] Complex **2** included an (*S*)- or (*R*)-phenylalanine derivative (*N*,*N*-bis(carboxymethyl)-(*S*)/(*R*)-phenylalanine, (*S*)/(*R*)-bcmpa) acting as the recognition site for the heme crevice of cyt *c* and disulfide linkages acting as anchors to the Au surface.

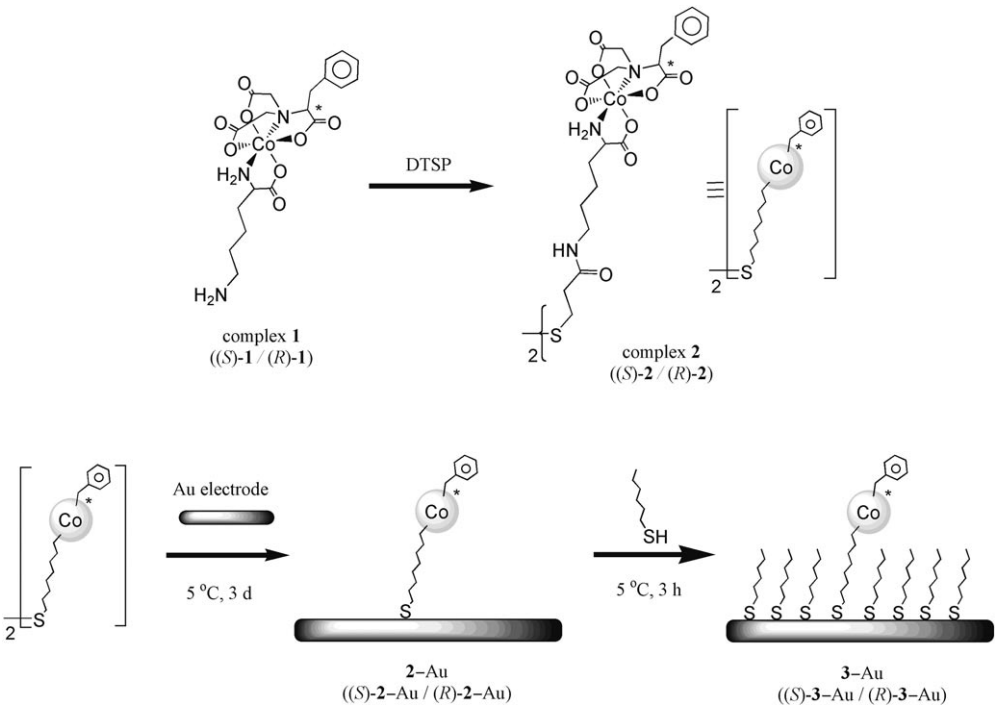

Scheme 1. Schematic view of complexes **1** and **2** and the preparation scheme for **2**–Au and **3**–Au. DTSP: Dithio bis(succinimidyl propionate).

The Co^{III} units were negatively charged (1−) for interaction with the positively charged surface of cyt *c*. A number of chiral-selective electron-transfer reactions between metalloproteins and optically active metal complexes have been explored,[35–40] but no optically active metal complex behaves like a promoter. We therefore examined the interaction between cyt *c* and the chiral benzyl group of the Co^{III} units through the promoting electron-transfer reaction between cyt *c* and the Au electrode. Indeed, the *S* or *R* configuration of the benzyl group of the Co^{III} unit of the Au electrode affected the association rate to cyt *c*, as estimated from cyclic voltammetry of cyt *c* by using **2**–Au and **3**–Au.[34] The electron-transfer characteristics were similar to those of intermolecular electron-transfer reactions between cyt c^{II} and $[Ru^{III}((S)$-/(R)-bcmpa)(bpy)] (bpy: 2,2′-bipyridine) in aqueous solution.[40d] These investigations suggested that the dependence of the electron-transfer behavior on the chirality of the complex arises from differences in steric interactions between the heme crevice of cyt *c* and the benzyl group of the Co^{III} units on the surface of the electrode.

Herein, we report the details of the preparation of a series of Co^{III} complex-modified monolayers and the redox behavior of cyt *c* as a function of the extent of surface coverage of the Co^{III} units on the Au electrode. The surface-coverage dependence of redox behavior provides clarification about the electron-transfer reaction through the association process between cyt *c* and the Co^{III} units of the SAMs. Moreover, it is demonstrated that the optically active Co^{III} complex-modified SAMs constructed in this study can detect local changes in structure induced by different oxidation states of cyt *c*.

Results and Discussion

Characterization and electrochemical properties of 1 and 2: (S)-**1** and (R)-**1** were synthesized from (S)- and (R)-phenylalanine derivatives, respectively. The synthesis of **1** produced two isomers originating from the coordination of (S)-lysine to the metal ion in the *trans*-(N) and *cis*-(N) forms. The *trans*-(N) form, obtained as the main product, was used in this study. Spectroscopic measurements and X-ray crystal structures have indicated that the side chain is constrained to the equatorial plane for both complexes.[41] The spectroscopic and electrochemical data are summarized in Table 1.

The UV/visible spectra of **1** indicate the presence of two *d*–*d* transition bands (Table 1, Figure S1 in the Supporting Information). These spectral data are similar to those obtained from spectral measurements of *trans*-(N)-K[$Co^{III}((S)$-bcmpa)$((S)$-phenylalanine)] (λ (ε) = 373 (170), 510 nm ($170\,M^{-1}\,cm^{-1}$)).[41] The CD spectral data for (S)-**1** are also similar to those of *trans*-(N)-K[$Co^{III}((S)$-bcmpa)$((S)$-phenylalanine)] (λ ($\Delta\varepsilon$) = 375 (+0.43), 485 (−1.14), 543 (+0.31), 609 nm ($+0.18\,M^{-1}\,cm^{-1}$)).[41] In the case of (R)-**1**, only the band near 610 nm, originating from a transition attributable to the chiral site, is inverted relative to that of (S)-**1**.

Table 1. UV/visible, CD, and electrochemical data for **1** and **2**.

	UV/visible[a] λ [nm] (ε [$M^{-1}\,cm^{-1}$])		CD[a] λ [nm] ($\Delta\varepsilon$ [$M^{-1}\,cm^{-1}$])			CV[b] E_{pc} [mV]
(S)-**1**	372 (160)	509 (150)	371 (+0.39)	484 (−1.0)	543 (+0.26)	610 (+0.25)	−450
(R)-**1**	372 (150)	509 (140)	371 (+0.28)	485 (−1.1)	–	613 (−0.34)	−448
(S)-**2**	372 (390)	509 (360)	371 (+0.81)	485 (−2.2)	542 (+0.46)	611 (+0.35)	−291
(R)-**2**	372 (380)	509 (350)	374 (+0.55)	489 (−2.5)	–	614 (−1.2)	−310

[a] 1 mM (in H_2O), l = 1 cm. [b] CV: cyclic voltammetry. 1 mM (in 0.1 M phosphate buffer (pH 7.0, I = 0.1 M ($NaClO_4$)).

Cyclic voltammograms of **1** and **2** were measured in 0.1 M phosphate buffer solution (pH 7.0) by using a glassy carbon electrode as the working electrode. The voltammogram of (R)-**2** is shown in Figure 1a. An irreversible reduction wave

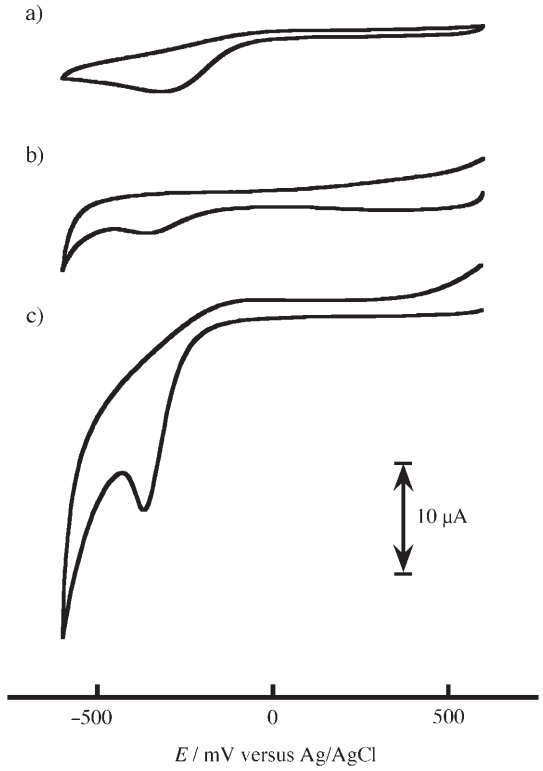

Figure 1. Cyclic voltammograms of a) (R)-**2**, b) (R)-**2**–Au prepared at 5 °C, and c) (R)-**2**–Au prepared at 25 °C in a phosphate buffer solution. (R)-**2**–Au was immersed for 3 d. The scan rate was $50\,mV\,s^{-1}$.

is observed at $E = -310$ mV versus Ag/AgCl (Table 1) and is assigned to $Co^{II/III}$ of (R)-**2**. The reduction potentials of (S)-**2** and (R)-**2** are similar to that of *trans*-(N)-K[$Co^{III}((S)$-bcmpa)$((S)$-phenylalanine)] ($E_{pc} = -330$ mV).[41] As a redox wave is not observed near the redox potential of cyt *c* (+55 mV),[3] the Co^{III} unit does not mediate an electron-transfer reaction between cyt *c* and the Au electrode in this redox range.[42] Cyclic voltammograms of cyt *c* in the pres-

ence of (*S*)-**1** (10 equiv) do not produce redox waves (Figure S2 in the Supporting Information). These results obviously suggest that the Co^{III} unit in aqueous solution cannot mediate and/or cannot promote heterogeneous electron-transfer reactions near the redox potential of cyt *c*.

Preparation of (*S*)-2/(*R*)-2–Au: Monolayer **2**–Au is prepared by dipping the Au electrode in a 1 mM aqueous solution of **2**. The surface coverage of **2**–Au is controlled by the immersion time and temperature. As both (*S*)-**2**–Au and (*R*)-**2**–Au exhibit similar coverage values under the same immersion conditions, only the case of (*R*)-**2**–Au will be discussed below.[43]

The cyclic voltammograms measured for (*R*)-**2**–Au in a phosphate buffer solution, immersed for three days at 5 or 25 °C, are shown in Figures 1b and c, respectively. Both voltammograms show the same irreversible reduction wave, which is similar to that of (*R*)-**2** (Figure 1a). As the reduction waves are not observed in the second cycles, these reduction waves are assigned to the reduction of the Co^{III} units. The reduction potentials of (*R*)-**2**–Au prepared under the two temperature conditions are similar (−360 mV), although these potentials are negatively shifted relative to the reduction potential of (*R*)-**2** (−310 mV). As the reduction to Co^{II} in the (*R*)-**2**–Au decreases the net charge from 1− to 2−, the negative shift is probably due to the electrostatic repulsion between Co units and/or the effect of a counter cation. The surface-coverage values of the Co units in (*R*)-**2**–Au, Γ_{Co}, were estimated from Equation (1), in which Q_{Co} is the quantity of electricity of the reduction peak in each voltammogram, n is the number of electrons, F is the Faraday constant, and A is the surface area of the Au electrode.

$$\Gamma_{Co} = Q_{Co}/(nFA) \quad (1)$$

The estimated Γ_{Co} values are 3.6×10^{-11} (at 5 °C) and 1.9×10^{-10} mol cm^{-2} (at 25 °C). The surface-coverage values representing the total number of Au–S bonds in (*R*)-**2**–Au, Γ_{des}, are 3.5×10^{-11} (at 5 °C) and 1.7×10^{-10} mol cm^{-2} (at 25 °C), as estimated from the reductive desorption waves in a 0.5 M KOH aqueous solution with freshly prepared (*R*)-**2**–Au.[44] The Γ_{Co} and Γ_{des} values are in good agreement at both temperatures. This result indicates that the reduction waves in the buffer solution and the desorption waves in the 0.5 M KOH aqueous solution are assignable to the reduction potentials of $Co^{II/III}$ and the desorption of Co units, respectively. (*R*)-**2**–Au immersed for three days at 25 °C exhibits Γ_{Co} and Γ_{des} values about fivefold larger than those for (*R*)-**2**–Au immersed for three days at 5 °C.

The surface-coverage values (Γ_{des}) of (*R*)-**2**–Au prepared at 5 and 25 °C are plotted against the length of time of immersion in Figure 2. At 25 °C (●), the surface-coverage values increase with increasing immersion times until saturation is reached at $1.7–1.9\times10^{-10}$ mol cm^{-2}. The calculated ideal surface coverage is 3.6×10^{-10} mol cm^{-2}, as estimated from the projected size of a Co^{III} unit. The saturated coverage value at 25 °C is close to this value, thereby indicating

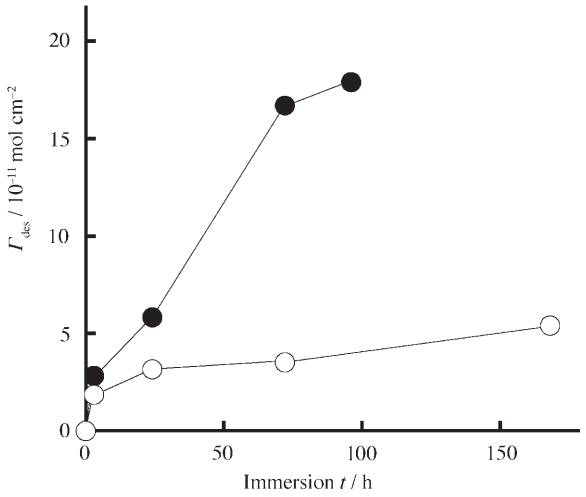

Figure 2. Plots of the extent of surface coverage of (*R*)-**2**–Au against the immersion time at 5 (○) and 25 °C (●).

that the (*R*)-**2** within (*R*)-**2**–Au is densely packed on the Au electrode. At 5 °C (○), the increase in coverage reaches apparent saturation after one to three days ($3.5–4.3\times10^{-11}$ mol cm^{-2}), but after seven days, the coverage increases slightly. The maximum coverage of (*R*)-**2**–Au at 5 °C is much lower. A two-step process for the molecular adsorption of SAMs has been proposed.[45] At first, the molecules are assembled by adsorption to the Au surface while they are lying flat. Further adsorption leads to dense packing by noncovalent interactions such as van der Waals interactions, hydrogen bonding, and π–π stacking. Thus, the coverage of (*R*)-**2**–Au prepared at the lower temperature is low because of stabilization of Co^{III} units adsorbed onto the Au surface with the molecules lying horizontally. This has probably been caused by the lower adsorption rates of (*R*)-**2** and/or the specific adsorption of the Co^{III} units onto the Au surface.

Redox behavior of cyt *c* depending upon the surface coverage of (*R*)-2–Au: Cyclic voltammograms of densely (approximately 2.0×10^{-10} mol cm^{-2}) and loosely (approximately 4.0×10^{-11} mol cm^{-2}) packed monolayers of (*R*)-**2** in phosphate buffer solution with or without cyt *c* are shown in Figure 3. In the absence of cyt *c*, a redox wave is not observed in this region. The redox wave of cyt $c^{II/III}$ is observed only in the case of the loosely packed monolayer. Its redox potential (+65 mV) is in agreement with the previously reported value of +55 mV.[3] As mentioned above, in the homogeneous system, **1** cannot promote electron transfer to cyt *c*; this clearly indicates that (*R*)-**2** adsorbed onto the Au surface can promote the electron-transfer reaction between cyt *c* and the Au electrode. It is notable that the electron-transfer reaction with cyt *c* is significantly dependent upon the surface coverage of (*R*)-**2**–Au. This type of coverage-dependent electron transfer has never been reported in a surface promoter system.[16–22] Indeed, a densely packed monolayer of 4-pyS exhibited the largest peak current of cyt *c*.[18c]

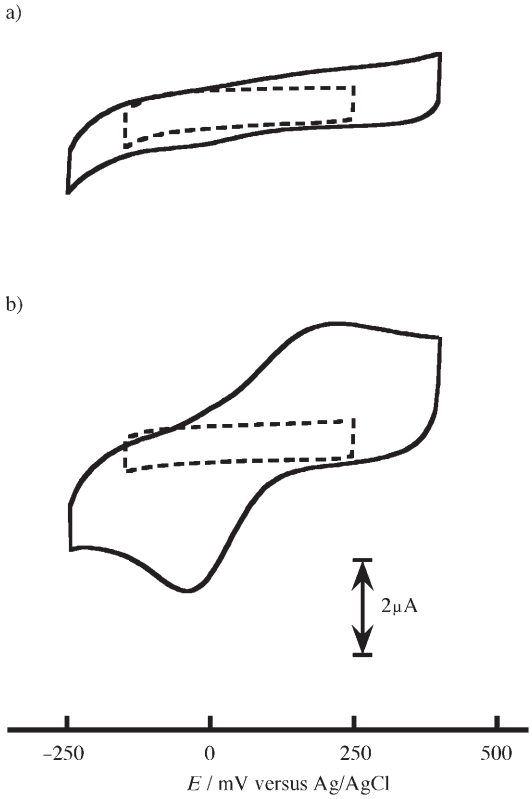

Figure 3. Cyclic voltammograms in a phosphate buffer solution (-----) and a cyt *c* solution (——), by using a) densely packed (approximately 2.0×10^{-10} mol cm^{-2}) and b) loosely packed (approximately 4.0×10^{-11} mol cm^{-2}) monolayers of (*R*)-**2**. The scan rate was 50 mV s^{-1}.

This result indicates that the electron-transfer mechanisms of (*R*)-**2**–Au with cyt *c* are quite different from those of any other promoter systems.

To study the surface-coverage dependence in detail, cyclic voltammograms of cyt *c* were measured by using a series of species of (*R*)-**2**–Au with varying surface coverages. Figure 4

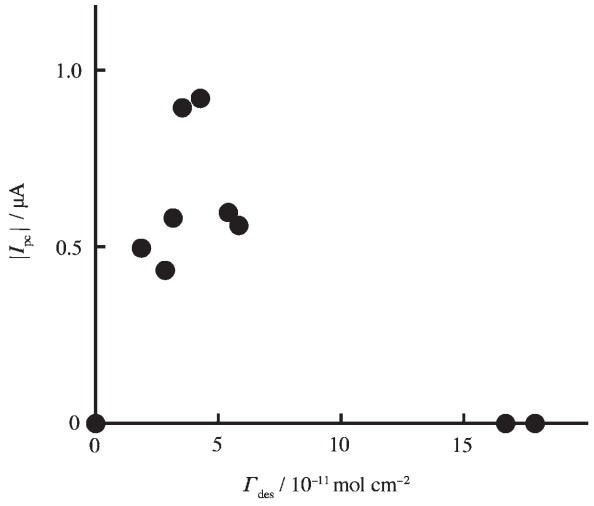

Figure 4. Plots of the cathodic peak current of cyt *c* ($v=10$ mV s^{-1}) against the surface coverage of (*R*)-**2**–Au.

shows the plots of the cathodic peak currents (I_{pc}) against surface coverages (Γ_{des}). When the coverage is about 4.0×10^{-11} mol cm^{-2}, the peak current of cyt *c* has the largest value. This result strongly suggests that an optimal surface coverage is necessary in order for cyt *c* to interact with the Co^{III} unit. The most favorable coverage is about 4.0×10^{-11} mol cm^{-2} (5 °C, 3 d) in this electron-transfer system. An increase in the coverage past this value causes a decrease in the peak current of the redox waves of cyt *c*. Thus, the electron transfer between cyt *c* and (*R*)-**2**–Au is particularly affected by the density of Co^{III} units on the surface.

Whitesides and co-workers reported that the binding rate between carbonic anhydrase (CA) and a mixed monolayer composed of arylsulfonamide (ASA) and tri(ethylene glycol) derivatives is strongly dependent on the molecular surface density of the ASA.[32,33] This dependence reflects the fact that the active site of the zinc ion in CA is located at a depth of 15 Å within the enzyme and also that the CA enzyme molecule is much larger than the ASA molecule. In the case of very low surface densities of ASA, the processes of binding and release of CA were highly reversible. The binding rates dramatically decreased when the density of ASA was larger than the optimal CA coverage estimated from the molecular size. In the case of much higher density coverages of ASA, the binding of CA did not occur. Steric repulsion among CA molecules was proposed as the cause of these observations.[33c]

This proposal may also explain the results of our coverage-dependent electron-transfer reaction between (*R*)-**2**–Au and cyt *c*. In our systems, the electron-transfer reactions occur through the associated complex between cyt *c* and the Co^{III} unit. Moreover, the benzyl group of the Co^{III} unit of (*R*)-**2**–Au would be expected to penetrate into the heme crevice of cyt *c*. The calculated ideal coverage of cyt *c* is 1.5×10^{-11} mol cm^{-2}, as estimated from the molecular size of cyt *c*.[25] In the case of the loosely packed monolayer (4.0×10^{-11} mol cm^{-2}), the ratio of Co^{III} units to one cyt *c* molecule is approximately 2, while it is approximately 10 in the case of the densely packed monolayer (2.0×10^{-10} mol cm^{-2}). The former results in effective electron transfer to cyt *c*, while the latter is essentially ineffective in promoting electron transfer. In the former case, cyt *c* associates effectively with (*R*)-**2** on the Au surface and the electron-transfer reaction between the electrode and cyt *c* is observed. On the other hand, the association of cyt *c* with (*R*)-**2** is negligible in the latter case. This causes poor association between the Co^{III} unit and cyt *c*, which results in ineffective electron transfer between the electrode and cyt *c*. The associated complexes proposed for our (*R*)-**2**–Au systems are schematically represented in Figure 5.

Electron-transfer behaviors of cyt *c* with 2–Au and 3–Au: Cyclic voltammograms of cyt *c* as measured with (*S*)-**2**–Au and (*R*)-**2**–Au are shown in Figure 6 and the electrochemical data are summarized in Table 2. Both SAMs were prepared by immersion for three days at 5 °C (approximately 4.0×10^{-11} mol cm^{-2}).[43] The redox waves of cyt $c^{II/III}$ were ob-

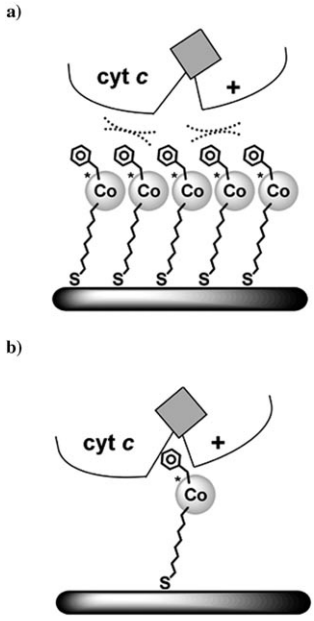

Figure 5. Schematic representations of associated complexes between cyt *c* and the Co^{III} unit with the a) densely packed (approximately 2.0×10^{-10} mol cm^{-2}) and b) loosely packed (approximately 4.0×10^{-11} mol cm^{-2}) monolayers of (*R*)-**2**.

served for both SAMs and became broader with increasing scan rates. These voltammograms are similar to sigmoidal-shaped curves (radial diffusion dominant), a result indicating that electron transfer occurs at some electroactive site on the electrode surface (the Co^{III} units in this system).[16d,19,46] However, the redox wave disappeared at a scan rate of 500 mV s^{-1}, which means that the rate-determining step in this system is probably not the diffusion process. In this case, it is difficult to apply theoretical radial diffusion directly. Thus, we need to focus on peak separation to estimate the overall electron-transfer rate in this system. The difference in peak separation between (*S*)-**2**–Au and (*R*)-**2**–Au at each scan rate, $\Delta(\Delta E_p)_{S-R}$, is defined as shown in Equation (2), in which $\Delta E_{p,S}$ and $\Delta E_{p,R}$ are the peak separations for (*S*)-**2**–Au and (*R*)-**2**–Au at each scan rate.

$$\Delta(\Delta E_p)_{S-R} = \Delta E_{p,S} - \Delta E_{p,R} \quad (2)$$

The $\Delta(\Delta E_p)_{S-R}$ values are plotted against scan rates (◆; Figure 7). At 10–50 mV s^{-1}, the $\Delta(\Delta E_p)_{S-R}$ values are almost zero, thereby indicating that the overall electron-transfer rates (k) are similar. However, when the scan rate exceeds 100 mV s^{-1}, the $\Delta(\Delta E_p)_{S-R}$ values gradually decrease ($\Delta E_{p,S} < \Delta E_{p,R}$). This observation clearly indicates that the overall electron-transfer rate between cyt *c* and (*S*)-**2**–Au is faster than that between cyt *c* and (*R*)-**2**–Au[47] and that the differences in the electron-transfer rates between (*S*)-**2**–Au and (*R*)-**2**–Au are quite sensitive to the scan rate. This scan-rate dependence of the $\Delta(\Delta E_p)_{S-R}$ value was also observed in the case of azurin-1, a blue copper protein, with **2**–Au.[48] In contrast, when $[Ru(NH_3)_6]^{3+}$ was employed instead of cyt *c*, both of the SAMs exhibited the same peak separations at each scan rate (Figure S3 in the Supporting Information). From these results, two important conclusions can be drawn: 1) The absolute configuration of the amino acid residue interacting with the Co^{III} unit in **2**–Au has an effect on the rate of electron transfer between the electrode and cyt *c*, and 2) **2**–Au promotes electron transfer with small and achiral molecules, such as $[Ru(NH_3)_6]^{3+}$, with no distinction of the absolute configuration of the amino acid.

The overall electron-transfer rate (k), estimated from the peak separation, is dependent on the diffusion (k_D), association (k_A), and electron-transfer rates (k_{ET}) of this system. As the structures of (*S*)-**2** and (*R*)-**2** are identical to each other

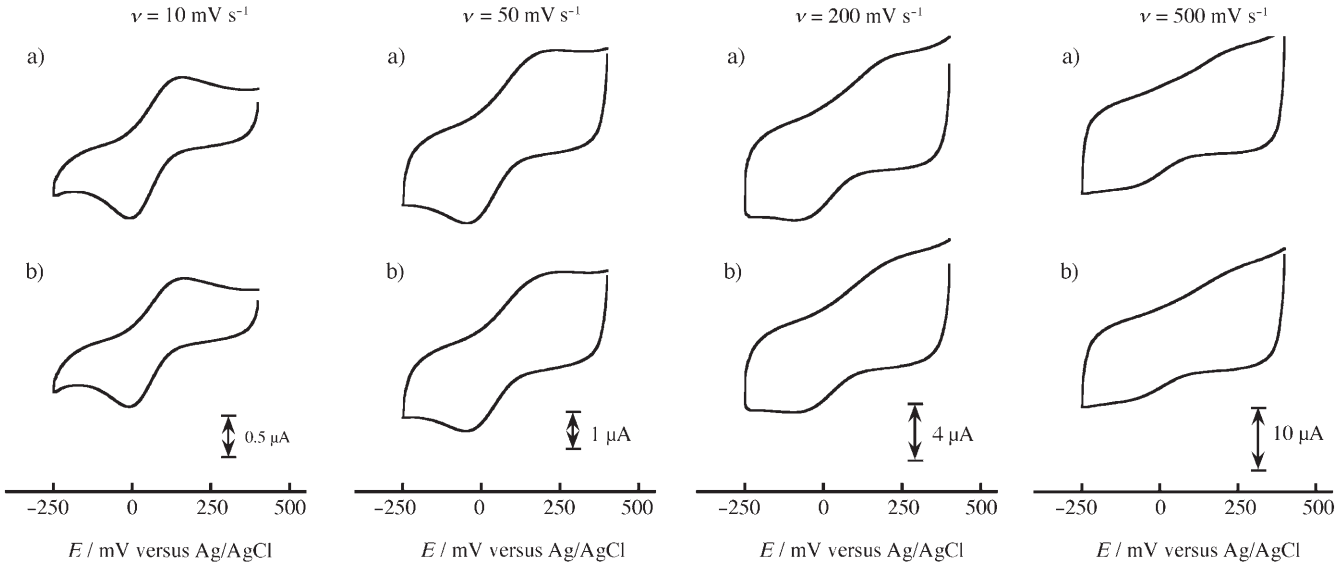

Figure 6. Cyclic voltammograms of cyt *c* with a) (*S*)-**2**–Au and b) (*R*)-**2**–Au at several scan rates (ν).

Table 2. Electrochemical parameters calculated from the voltammograms of cyt *c* with (*S*)-**2**–Au and (*R*)-**2**–Au.[a]

	(*S*)-**2**–Au			(*R*)-**2**–Au					
v[b]	E_{pc}[c] ($\lvert shift \rvert_{pc}$[d])	E_{pa}[c] ($\lvert shift \rvert_{pa}$[d])	ΔE_p[e]	E_{pc}[c] ($\lvert shift \rvert_{pc}$[d])	E_{pa}[c] ($\lvert shift \rvert_{pa}$[d])	ΔE_p[e]	Δ_{S-R} $\Delta(\Delta E_p)$[f]	$\Delta(\lvert shift \rvert_{pc})$[g]	$\Delta(\lvert shift \rvert_{pa})$[g]
10	−8 (0)	+137 (0)	145	−3 (0)	+141 (0)	144	+1	0	0
25	−24 (16)	+164 (27)	188	−20 (17)	+170 (29)	190	−2	−1	−2
50	−40 (32)	+186 (49)	226	−39 (36)	+187 (46)	226	0	−4	+3
100	−49 (41)	+181 (44)	230	−50 (47)	+205 (64)	255	−25	−6	−20
200	−79 (71)	+204 (67)	283	−78 (75)	+230 (89)	308	−25	−4	−22
300	−84 (78)	+209 (72)	293	−85 (82)	+268 (127)	353	−60	−4	−55
400	−126 (118)	+232 (95)	358	−135 (132)	+304 (163)	439	−81	−14	−68

[a] [cyt *c*] = 100 μM (in 0.1 M phosphate buffer (pH 7.0, I = 0.1 M ($NaClO_4$))). [b] v: scan rate [mV s^{-1}] [c] Cathodic and anodic peak potentials [mV versus Ag/AgCl]. [d] $\lvert shift \rvert_{pc} = \lvert E_{pc}(n) - E_{pc}(10) \rvert$, $\lvert shift \rvert_{pa} = \lvert E_{pa}(n) - E_{pa}(10) \rvert$, n = 10–400 [mV]. [e] ΔE_p: peak separation [mV]. [f] $\Delta(\Delta E_p)_{S-R} = \Delta E_{p,S} - \Delta E_{p,R}$ [mV]. [g] $\Delta(\lvert shift \rvert_{pc})_{S-R} = \lvert shift \rvert_{pc,S} - \lvert shift \rvert_{pc,R}$, $\Delta(\lvert shift \rvert_{pa})_{S-R} = \lvert shift \rvert_{pa,S} - \lvert shift \rvert_{pa,R}$ [mV].

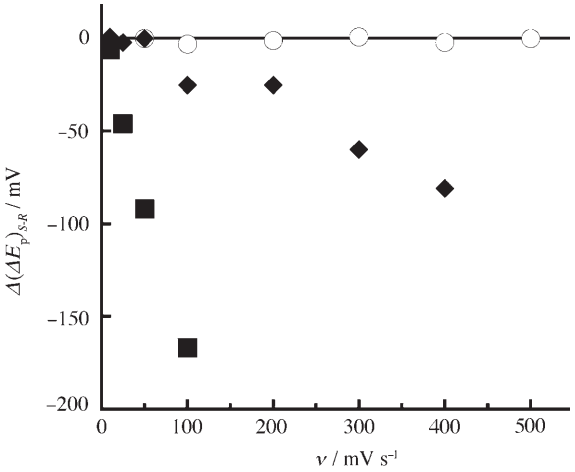

Figure 7. The relationship between scan rates (v) and $\Delta(\Delta E_p)_{S-R}$ values for **2**–Au–cyt *c* (◆), **3**–Au–cyt *c* (■), and **3**–Au–$[Ru(NH_3)_6]^{3+}$ (○) systems.

and their SAMs give similar coverages,[43] the value of k_D for **2**–Au is probably not affected by its *S* or *R* configuration.[46] Therefore, it does not influence the $\Delta(\Delta E_p)_{S-R}$ value. When the associated structure of the Co^{III} unit and cyt *c* is distinct as a result of the *S* or *R* configuration of **2**, the values of k_{ET} for (*S*)-**2**–Au and (*R*)-**2**–Au may be different. However, the k_{ET} values are intrinsically independent of scan rates. Moreover, at slow scan rates, the $\Delta(\Delta E_p)_{S-R}$ values are almost zero. As the values of k_{ET} may also be similar between (*S*)-**2**–Au and (*R*)-**2**–Au, the associated structures are not affected by the *S* or *R* configuration. Thus, only the value of k_A is affected by scan rates. The scan-rate dependence of $\Delta(\Delta E_p)_{S-R}$ shown in Figure 7 originates from the difference in the rate of association (k_A) induced by the *S* or *R* configuration of **2**. This dependence is influenced by the fit of the benzyl group on the Co^{III} unit of **2**–Au into the heme crevice of cyt *c*. Thus, cyt *c* strictly recognizes the orientation of the benzyl group on the electrode surface through the association process. The proposed electron-transfer mechanisms with cyt *c* are schematically represented in Figure 8.

Monolayer **3**–Au, which has a mixed monolayer composed of **2** and hexanethiol, was prepared to investigate the effect of alteration of the gap between the molecules of **2** in **2**–Au. The background current of **3**–Au caused by double-layer charging was smaller than that of **2**–Au. This result suggests

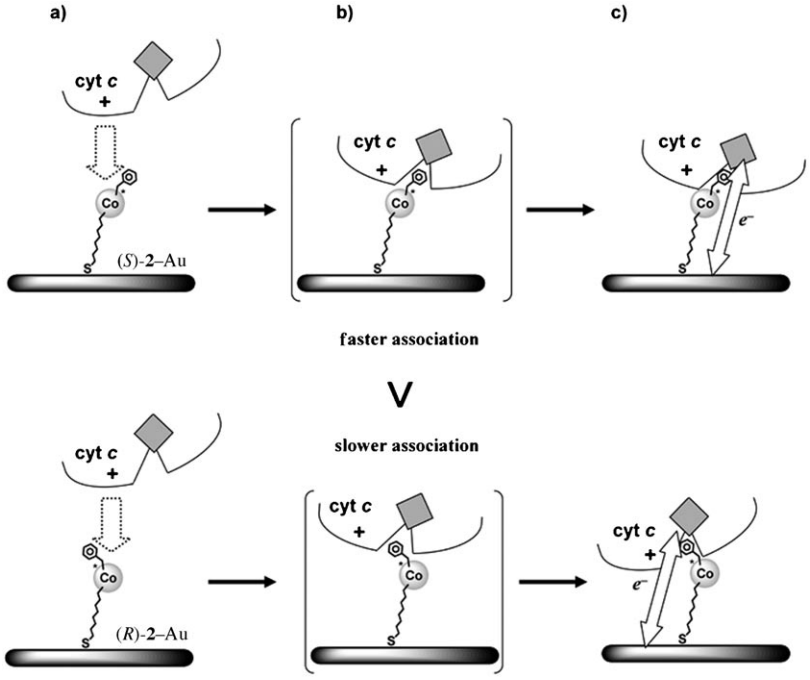

Figure 8. Schematic representation of the proposed mechanism for the electron-transfer reaction of cyt *c* with (*S*)-**2**–Au (top) and (*R*)-**2**–Au (bottom). a) Diffusion: positively charged cyt *c* approaches the negatively charged electrode surface and then adsorbs the Co^{III} unit electrostatically. b) Association: adsorbed cyt *c* moves and/or rotates on the Au surface to form the associated structure with a Co^{III} unit. The association process is probably affected by slight structural differences induced by the chirality of the Co^{III} unit. c) Electron transfer: cyt $c^{II/III}$ donates/accepts an electron to/from the Au electrode as appropriate.

that **3**–Au forms a more densely packed monolayer than **2**–Au.[49] The redox waves of cyt $c^{II/III}$ are clearly observed, as in the case of **2**–Au (Figure S4 and Table S1 in the Supporting Information). As shown in Figure 7, the $\Delta(\Delta E_p)_{S-R}$ values of **3**–Au are dependent on the scan rate and the behavior is similar to that of **2**–Au. It is notable that the $\Delta(\Delta E_p)_{S-R}$ values of **3**–Au indicate a larger difference with slow scan rates (10–50 mV s^{-1}), whereas **2**–Au showed no significant differences in this range. As the motion of the Co^{III} units in **3**–Au is restricted by hexanethiols filling the gap among the Co^{III} units, the larger difference in the k_A values may be induced by the *S* or *R* configuration, relative to that which occurs in the case of **2**–Au.

Recognition behavior between the reduction and oxidation of cyt *c*: The $|E_{pa}-E_{pa/2}|$ and $|E_{pc}-E_{pc/2}|$ values of cyt *c* were estimated to be 89 and 62 mV, respectively, from the voltammogram of cyt *c* at a scan rate of 10 mV s^{-1} with (*R*)-**2**–Au at a coverage of 4.0×10^{-11} mol cm^{-2}.[50] The theoretical value of $|E_p-E_{p/2}|$ is 56.5 mV for a fully reversible system.[47] Thus, this result indicates that the oxidation rate of cyt c^{II} is lower than the reduction rate of cyt c^{III}. At 10 mV s^{-1}, the ΔE_p values for (*S*)-**2**–Au and (*R*)-**2**–Au are similar; therefore, the absolute configuration of the Co^{III} unit is not affected by the ΔE_p value at this scan rate. In order to separate the differences induced by the *S* and *R* configurations of the Co^{III} unit, the shifts from the peak potentials at 10 mV s^{-1}, $|\text{shift}|_{pa}$ and $|\text{shift}|_{pc}$, and the differences between **2**–Au (or **3**–Au), $\Delta(|\text{shift}|_{pa})_{S-R}$ and $\Delta(|\text{shift}|_{pc})_{S-R}$, were defined as shown in Equations (3) and (4), in which $E_{pa}(10)$, $E_{pc}(10)$, $E_{pa}(n)$, and $E_{pc}(n)$ are the anodic and cathodic peak potentials at 10 and *n* (10–400 mV s^{-1}), respectively.[51]

$$|\text{shift}|_{pa} = |E_{pa}(n)-E_{pa}(10)|,\ |\text{shift}|_{pc} = |E_{pc}(n)-E_{pc}(10)| \quad (3)$$

$$\begin{aligned}\Delta(|\text{shift}|_{pa})_{S-R} &= |\text{shift}|_{pa,S}-|\text{shift}|_{pa,R},\\ \Delta(|\text{shift}|_{pc})_{S-R} &= |\text{shift}|_{pc,S}-|\text{shift}|_{pc,R}\end{aligned} \quad (4)$$

Figure 9 shows the relationship between scan rates and the values of $\Delta(|\text{shift}|_{pa})_{S-R}$ and $\Delta(|\text{shift}|_{pc})_{S-R}$. Both values are near zero in the case of the **3**–Au–$[Ru(NH_3)_6]^{3+}$ system. In the anodic reaction (oxidation of cyt c^{II}; Figure 9a), the behavior of $\Delta(|\text{shift}|_{pa})_{S-R}$ is similar to that of $\Delta(\Delta E_p)_{S-R}$. In the cathodic reaction (reduction of cyt c^{III}; Figure 9b), the $\Delta(|\text{shift}|_{pc})_{S-R}$ values are near zero in the case of the **2**–Au–cyt *c* system. In the **3**–Au–cyt *c* system, the $\Delta(|\text{shift}|_{pc})_{S-R}$ values are slightly negative. The redox potential of the Co^{III} units (−360 mV) is out of range under these experimental conditions. Thus, structural and/or conformational changes of the Co^{III} unit do not occur upon association with cyt *c* during the electron-transfer reaction. These results strongly suggest that differences in the oxidation states of cyt *c* affect the recognition of the benzyl group of the Co^{III} unit in **2**–Au and **3**–Au. The cyt c^{II} state associates more strongly with the benzyl group than the cyt c^{III} state.

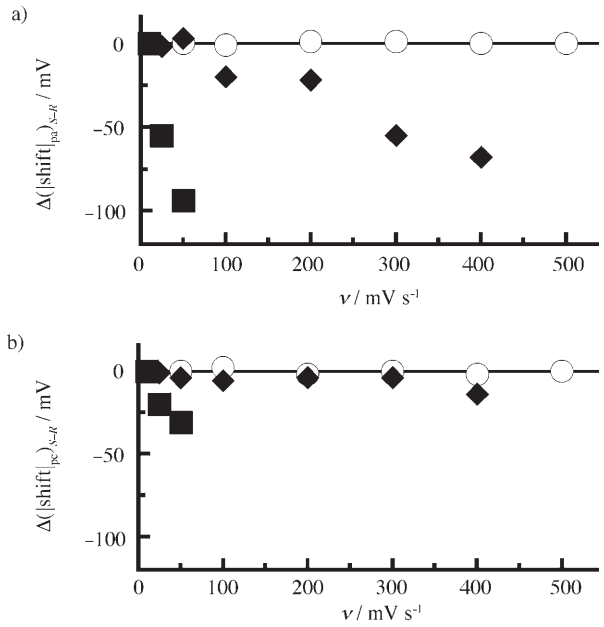

Figure 9. Plots of a) $\Delta(|\text{shift}|_{pa})_{S-R}$ and b) $\Delta(|\text{shift}|_{pc})_{S-R}$ against scan rates for **2**–Au–cyt *c* (◆), **3**–Au–cyt *c* (■), and **3**–Au–$[Ru(NH_3)_6]^{3+}$ (○) systems.

The difference in the oxidation states of cyt *c* is considered to have caused the change in the structural environment around the heme crevice. In the case of reduction of cyt c^{III}, the heme crevice of cyt c^{III} spreads and its association with the Co^{III} unit is weakened. Conversely, strong association of the Co^{III} unit occurs upon oxidation of cyt c^{II} because the heme crevice becomes narrower. This observation of stronger association is also observed in the aqueous electron-transfer reaction between Ru^{III} complexes (whose structure is similar to **1**) and cyt c^{II}.[40d] In this case, the second-order rate constant of $[Ru^{III}((S)\text{-bcmpa})(bpy)]$ is larger than that of the *R* enantiomer. The surface area of heme exposed to solvent was calculated to be 14.6 % for cyt c^{III} and 7.53 % for cyt c^{II}, as determined by a ^{1}H NMR spectroscopic study.[52] These results provide strong support for our interpretation that the size of the heme crevice is regulated by the difference in the oxidation state of cyt *c*. Therefore, our electrodes, **2**–Au and **3**–Au, can indirectly determine the size of the heme crevice for cyt $c^{II/III}$. As mentioned above, cyt *c* must dissociate from its redox partners after the *exergonic* electron-transfer reaction through the associated complex in vivo. It has been proposed hitherto that the conformational change in each oxidation state of cyt *c* provides the driving force for the dissociation process.[53–55] It is difficult to detect structural differences in examples of flat and well-ordered monolayers by using promoter molecules.[16–22] In fact, in the case of 4,4′-bipyridine, the kinetic parameters of the reduction and oxidation reactions of cyt *c*, which were estimated by using rotating-disk and ring-disk electrodes, showed no difference.[56] Our chiral Co^{III} complex-modified SAM system has the ability to detect changes in the size of the heme crevice through electrochemical measurements.

Conclusion

We prepared SAMs of optically active Co^{III} complex **2**, which includes a molecular recognition site, and thoroughly investigated their electron-transfer behavior with cyt *c*. Various surface coverages are obtained for **2**–Au as a result of varying the immersion time and temperature. The largest peak current of cyt *c* is obtained with a coverage of approximately 4.0×10^{-11} mol cm^{-2}. The peak currents dramatically decrease when the coverage exceeds this value. This coverage-dependent electron-transfer behavior suggests the existence of a defined process of association between cyt *c* and a Co^{III} unit for **2**–Au. The absolute configurations of the Co^{III} units in **2**–Au and **3**–Au (in which the latter has a mixed monolayer and the gaps are filled by hexanethiol) lead to different values of ΔE_p for cyt *c* at the same scan rate. As these results originate from differences in the association rates between the *S* and *R* configurations, our system is capable of detecting slight differences in structural interactions between the benzyl group on the Co^{III} unit and the heme crevice of cyt *c*. The association rate of **3**–Au is larger than that of **2**–Au, because hexanethiols constrain the Co^{III} units in **3**–Au. A difference in the association rates between **2**–Au and **3**–Au with cyt *c* was clearly observed during the oxidation of cyt c^{II} relative to the reduction of cyt c^{III}. Therefore, it is suggested that the size of the heme crevice of cyt c^{III} is comparatively wider than that of cyt c^{II}.

Our chiral Co^{III}-unit-modified electrodes are capable of detecting slight structural changes in the vicinity of the heme through electrochemical measurements. We are presently applying our SAMs with other electron-transfer proteins such as azurins and preparing new SAMs modified by similar Co^{III} complexes that include other amino acid mimetics. The further development of new SAMs is expected to provide a powerful tool for the investigation of the structure of the protein environment in the vicinity of metal centers in metalloproteins.

Experimental Section

Materials: All chemicals and solvents were purchased from Wako Pure Chemical Industries, Tokyo Chemical Industry, Nacalai Tesque, and Peptide Institute. All reagents were used without further purification. Milli-Q water was prepared by using a Milli-Q biocel A (Millipore). QAE Sephadex A-25 (Pharmacia, Cl^- form) was used for column chromatography. An Au wire (Niraco, $\varnothing=0.30$ mm) and an Au sheet (Niraco, thickness = 0.1 mm) were used for the preparation of the gold electrode. The (*S*)- and (*R*)-phenylalanine derivatives, (*S*)- and (*R*)-bcmpa, were synthesized according to previously reported methods.[57]

General procedures: UV/Visible and circular dichroism (CD) spectra were measured with a Ubest V-570 spectrophotometer (JASCO) and a J-820 spectrophotometer (JASCO) with a 1 cm pass-length quartz cell, respectively. All measurements were performed in aqueous solution at room temperature. ^{1}H NMR spectra were recorded with an AVANCE-600 spectrometer (Bruker) in D_2O. The chemical shifts (δ) are given in ppm relative to the signal for sodium 2,2′-dimethyl-2-silapentane-5-sulfonate (DSS) as an internal standard. Electrospray ionization/time of flight (ESI-TOF) mass spectra were obtained with a LCT ESI-TOF spectrometer (Micromass).

Complexes (*S*)-1 and (*R*)-1: The synthesis of (*S*)-**1** and (*R*)-**1** was based on the modification of a previously reported method.[58] $CoCl_2\cdot6H_2O$ (1.2 g, 5 mmol) and an aqueous solution of 30% H_2O_2 (2 mL) were dissolved in H_2O (10 mL). This solution was gradually added to $KHCO_3$ (3.5 g, 35 mmol) in aqueous solution (30 mL) with stirring in an ice bath. After filtration, (*S*)- or (*R*)-bcmpa (1.55 g, 5.5 mmol) in an aqueous solution (50 mL) neutralized with KOH was added to the filtered solution. After the mixture had been stirred at room temperature overnight, (*S*)-lysine·HCl (0.91 g, 5 mmol) in an aqueous solution (10 mL) neutralized with KOH was added to the resultant mixture with a small amount of active charcoal. The mixture was then stirred at 50 °C for 6 h with the pH value kept at 7 by addition of HCl. After filtration, the solution was evaporated and desalted with MeOH several times. The resultant residue was purified by column chromatography (QAE Sephadex A-25). A reddish-violet band was eluted with an aqueous solution (no ionic strength). The eluted solution was evaporated and desalted with MeOH. The residue was purified over QAE Sephadex A-25 again at a quite slow rate. The bluish-violet and reddish-violet bands were eluted with an aqueous solution (no ionic strength). The reddish-violet solution was evaporated and precipitated in MeOH. The reddish-violet powder was collected and dried in vacuo. The yields were 358 mg (15%) for (*S*)-**1** and 188 mg (7.8%) for (*R*)-**1**. ^{1}H NMR (600 MHz, D_2O): $\delta=1.68$–1.74 (m, 2H; lysine), 1.74–1.84 (m, 2H; lysine), 1.89–1.95 (m, 1H; lysine), 2.02–2.08 (m, 1H; lysine), 3.06 (t, 2H, J = 7.3 Hz; lysine), 3.24 (d, 1H, J = 16.6 Hz; bcmpa), 3.50 (dd, 1H, J = 4.6, 15.1 Hz; bcmpa), 3.62 (dd, 1H, J = 10.1, 15.1 Hz; bcmpa), 3.88 (dd, 1H, J = 4.5, 8.2 Hz; lysine), 3.95 (d, 1H, J = 18.1 Hz; bcmpa), 4.18 (d, 1H, J = 16.6 Hz; bcmpa), 4.61 (d, 1H, J = 18.1 Hz; bcmpa), 5.03 (dd, 1H, J = 5.5, 10.4 Hz; bcmpa), 7.44 (t, 1H, J = 7.6 Hz; bcmpa), 7.52 (t, 2H, J = 7.9 Hz; bcmpa), 7.61 ppm (d, 2H, J = 7.8 Hz; bcmpa); MS (ESI-TOF): m/z: 569.0 $[M-H^+]^-$; elemental analysis: calcd (%) for (*S*)-**1**·2.5H_2O ($C_{19}H_{31}N_3CoO_{10.5}$): C 43.19, H 5.91, N 7.95; found: C 43.04, H 5.84, N 8.16; calcd for (*R*)-**1**·2H_2O ($C_{19}H_{30}N_3CoO_{10}$): C 43.94, H 5.82, N 8.09; found: C 44.07, H 5.55, N 8.02.

Complexes (*S*)-2 and (*R*)-2: Complex (*S*)-**1** or (*R*)-**1** (48.3 mg, 0.1 mmol) was dissolved in a small amount of an aqueous solution of 0.1 M KCl, and the solvent was then evaporated completely. The resultant residue was dissolved in dimethylsulfoxide (DMSO) and neutralized with triethylamine (0.01 g, 0.1 mmol). A solution of DTSP (20.2 mg, 0.05 mmol) in DMSO (10 mL) was added to this mixture with stirring. After being stirred for 3 h at room temperature, the solution was evaporated completely and desalted with MeOH several times. The resulting residue was precipitated in H_2O/EtOH to yield a reddish-violet powder. The powder was collected and then dried in vacuo. The yields were 24.8 mg (46%) for (*S*)-**2** and 18.9 mg (31%) for (*R*)-**2**: ^{1}H NMR (600 MHz, D_2O): $\delta=$ 1.55–1.66 (m, 8H; lysine), 1.82–1.91 (m, 2H; lysine), 1.95–2.03 (m, 2H; lysine), 2.63 (t, 4H, J = 6.9 Hz; DTSP), 2.92 (t, 4H, J = 6.8 Hz; DTSP), 3.23 (d, 2H, J = 16.7 Hz; bcmpa), 3.24 (s, 4H; lysine), 3.49 (dd, 2H, J = 4.4, 14.9 Hz; bcmpa), 3.60 (dd, 2H, J = 10.0, 14.9 Hz; bcmpa), 3.83 (dd, 2H, J = 4.7, 8.6 Hz; lysine), 3.94 (d, 2H, J = 18.2 Hz; bcmpa), 4.15 (d, 2H, J = 16.7 Hz; bcmpa), 4.59 (d, 2H, J = 18.2 Hz; bcmpa), 5.01 (dd, 2H, J = 5.0, 10.3 Hz; bcmpa), 7.43 (t, 2H, J = 7.3 Hz; bcmpa), 7.50 (t, 4H, J = 7.4 Hz; bcmpa), 7.60 ppm (d, 4H, J = 7.5 Hz; bcmpa); MS (ESI-TOF): m/z: 569.0 $[M-2K]^{2-}$; elemental analysis: calcd for (*S*)-**2**·4H_2O ($C_{44}H_{64}N_6Co_2K_2O_{22}S_2$): C 40.99, H 5.00, N 6.52; found: C 40.83, H 5.14, N 6.40; calcd for (*R*)-**2**·5H_2O ($C_{44}H_{66}N_6Co_2K_2O_{23}S_2$): C 40.43, H 5.09, N 6.43; found: C 40.34, H 4.81, N 6.34.

Electrode preparation: A polycrystalline Au flag electrode was prepared by spot welding between an Au wire ($\varnothing=0.3$ mm) and an Au sheet (thickness = 0.1 mm, $\varnothing=6$ mm). The Au electrode was cleaned by boiling in mixed acid for 30 min and sonication in Milli-Q water. After annealing had been performed with a hydrogen flame, the electrode was quenched with Milli-Q water saturated with hydrogen.

Monolayers (*S*)-**2**–Au and (*R*)-**2**–Au were prepared by dipping the pretreatment Au electrode in an aqueous solution of 1 mM (*S*)-**2** or (*R*)-**2**, respectively, for various lengths of time at each temperature. (*S*)-**3**–Au and (*R*)-**3**–Au were obtained by dipping (*S*)-**2**–Au or (*R*)-**2**–Au, respectively, which had been prepared at 5 °C for 3 d, in a MeOH solution of approximately 1 mM hexanethiol for 3 h at 5 °C. These modified electrodes were

rinsed with water and/or MeOH solution before electrochemical measurements.

The surface area of the electrode was determined by the reduction of AuO (444 $\mu C\,cm^{-2}$) in an aqueous solution of 0.1 M H_2SO_4 ($A = 0.796\ cm^2$, roughness factor: 1.36).[59]

Electrochemical measurements: Electrochemical measurements were performed by using a CV-50W (BAS) and an HZ-5000 automatic polarization system (HOKUTO DENKO). The cyclic voltammetry and linear-sweep voltammetry were performed by using a glassy carbon or each SAM as a working electrode, with Pt wire as the counter electrode and Ag/AgCl (3 M NaCl) as the reference electrode. Ar gas was passed through the electrolyte solution for at least 15 min before each measurement.

The voltammetry measurements were performed in a 0.1 M phosphate buffer solution (pH 7.0, $I = 0.1$ M $NaClO_4$) or a 0.5 M KOH aqueous solution. A 1 mM $[Ru^{III}(NH_3)_6]Cl_3$ solution was prepared in the same buffer solution. A 100 μM horse heart cyt *c* (purchased from Nacalai Tesque) solution was prepared by dialyzing in the same buffer solution for a few times before use.[18]

Acknowledgements

This work was supported partly by a Grant-in-Aid for Scientific Research from the Ministry of Education, Science, Sports, and Culture of Japan and in part by a grant from the NITECH 21st Century COE Program.

[1] J. M. Anderson, B. Anderson, *Trends Biochem. Sci.* **1988**, *13*, 351–355.
[2] R. Huber, *Angew. Chem.* **1989**, *101*, 849–871; *Angew. Chem. Int. Ed. Engl.* **1989**, *28*, 848–869.
[3] *Cytochrome c: A Multidisciplinary Approach* (Eds.: R. A. Scott, A. G. Mauk), University Science Books, Sausalito, CA, **1996**.
[4] a) S. Takemori, K. Wada, K. Ando, M. Hosokawa, I. Sekuzu, K. Okunuki, *J. Biochem.* **1962**, *52*, 28–37; b) S. Takemori, K. Wada, I. Sekuzu, K. Okunuki, *Nature* **1962**, *195*, 456–457; c) K. Wada, K. Okunuki, *J. Biochem.* **1968**, *64*, 667–681; d) K. Wada, K. Okunuki, *J. Biochem.* **1969**, *66*, 263–272.
[5] M. Erecińska, J. S. Davis, D. F. Wilson, *J. Biol. Chem.* **1980**, *255*, 9653–9658.
[6] a) H. T. Smith, A. J. Ahmed, F. Millet, *J. Biol. Chem.* **1981**, *256*, 4984–4990; b) F. Millet, C. de Jong, L. Paulson, R. A. Capaldi, *Biochemistry* **1983**, *22*, 546–552.
[7] a) E. Margoliash, S. Ferguson-Miller, J. Tulloss, C. H. Kang, B. A. Feinberg, D. L. Brautigan, M. Morrison, *Proc. Natl. Acad. Sci. USA* **1973**, *70*, 3245–3249; b) S. Ferguson-Miller, D. L. Brautigan, E. Margoliash, *J. Biol. Chem.* **1976**, *251*, 1104–1115.
[8] R. Rieder, H. R. Bosshard, *J. Biol. Chem.* **1980**, *255*, 4732–4739.
[9] B. W. König, J. Wilms, B. F. van Gelder, *Biochim. Biophys. Acta* **1981**, *636*, 9–16.
[10] a) J. Butler, D. M. Davies, A. G. Sykes, W. H. Koppenol, N. Osheroff, E. Margoliash, *J. Am. Chem. Soc.* **1981**, *103*, 469–471; b) J. Butler, S. K. Chapman, D. M. Davis, A. G. Sykes, S. H. Speck, N. Osheroff, E. Margoliash, *J. Biol. Chem.* **1983**, *258*, 6400–6404; c) G. D. Armstrong, J. A. Chambers, A. G. Sykes, *J. Chem. Soc. Dalton Trans.* **1986**, 755–758.
[11] a) J. V. McArdle, H. B. Gray, C. Creutz, N. Sutin, *J. Am. Chem. Soc.* **1974**, *96*, 5737–5741; b) S. Wherland, H. B. Gray, *Proc. Natl. Acad. Sci. USA* **1976**, *73*, 2950–2954; c) J. V. McArdle, K. Yocom, H. B. Gray, *J. Am. Chem. Soc.* **1977**, *99*, 4141–4145; d) D. Cummins, H. B. Gray, *J. Am. Chem. Soc.* **1977**, *99*, 5158–5167; e) A. G. Mauk, C. L. Coyle, E. Bordignon, H. B. Gray, *J. Am. Chem. Soc.* **1979**, *101*, 5054–5056.
[12] a) J. F. Wishart, R. van Eldik, J. Sun, C. Su, S. S. Isied, *Inorg. Chem.* **1992**, *31*, 3986–3989; b) M. Meier, R. van Eldik, *Inorg. Chim. Acta* **1994**, *225*, 95–101; c) M. Meier, J. Sun, J. F. Wishart, R. van Eldik, *Inorg. Chem.* **1996**, *35*, 1564–1570; d) M. Meier, R. van Eldik, *Chem. Eur. J.* **1997**, *3*, 39–46; e) J. Macyk, R. van Eldik, *J. Chem. Soc. Dalton Trans.* **2001**, 2288–2292; f) D. Chatterjee, M. S. A. Hamza, M. M. Shoukry, A. Mitra, S. Deshmukh, R. van Eldik, *Dalton Trans.* **2003**, 203–209; g) J. Macyk, R. van Eldik, *Dalton Trans.* **2003**, 2704–2709; h) M. Körner, P. A. Tregloan, R. van Eldik, *Dalton Trans.* **2003**, 2710–2717.
[13] H. Pelletier, J. Kraut, *Science* **1992**, *258*, 1748–1755.
[14] C. Lange, C. Hunte, *Proc. Natl. Acad. Sci. USA* **2002**, *99*, 2800–2805.
[15] G. W. Bushnell, G. V. Louie, G. D. Brayer, *J. Mol. Biol.* **1990**, *214*, 585–595.
[16] a) M. J. Eddowes, H. A. O. Hill, *J. Chem. Soc. Chem. Commun.* **1977**, 771–772; b) M. J. Eddowes, H. A. O. Hill, *J. Am. Chem. Soc.* **1979**, *101*, 4461–4464; c) P. M. Allen, H. A. O. Hill, N. J. Walton, *J. Electroanal. Chem.* **1984**, *178*, 69–86; d) F. A. Armstrong, A. M. Bond, H. A. O. Hill, I. S. M. Psalti, C. G. Zoski, *J. Phys. Chem.* **1989**, *93*, 6485–6493; e) H. A. O. Hill, N. I. Hunt, A. M. Bond, *J. Electroanal. Chem.* **1997**, *436*, 17–25; f) J. J. Davis, H. A. O. Hill, A. M. Bond, *Coord. Chem. Rev.* **2000**, *200–202*, 411–442.
[17] M. Fedurco, *Coord. Chem. Rev.* **2000**, *209*, 263–331.
[18] a) I. Taniguchi, K. Toyosawa, H. Yamaguchi, K. Yasukouchi, *J. Chem. Soc. Chem. Commun.* **1982**, 1032–1033; b) I. Taniguchi, K. Toyosawa, H. Yamaguchi, K. Yasukouchi, *J. Electroanal. Chem.* **1982**, *140*, 187–193; c) I. Taniguchi, M. Kajiwara, T. Kai, R. Muraguchi, K. Tonemura, K. Nishiyama, *Chem. Sens.* **1993**, *9 (Suppl. B)*, 239–242; d) I. Taniguchi, S. Yoshimoto, K. Nishiyama, *Chem. Lett.* **1997**, 353–354; e) T. Sawaguchi, F. Mizutani, S. Yoshimoto, I. Taniguchi, *Electrochim. Acta* **2000**, *45*, 2861–2867.
[19] a) A. M. Bond, H. A. O. Hill, D. J. Page, I. S. M. Psalti, N. J. Walton, *Eur. J. Biochem.* **1990**, *191*, 737–742; b) A. M. Bond, H. A. O. Hill, S. Komorsky-Lovrić, M. Lovrić, M. E. McCarthy, I. S. M. Psalti, N. J. Walton, *J. Phys. Chem.* **1992**, *96*, 8100–8105.
[20] a) I. C. N. Diógenes, F. C. Nart, M. L. A. Temperini, I. S. Moreira, *Inorg. Chem.* **2001**, *40*, 4884–4889; b) P. Corio, G. F. S. Andrade, I. C. N. Diógenes, I. S. Moreira, F. C. Nart, M. L. A. Temperini, *J. Electroanal. Chem.* **2002**, *520*, 40–46; c) I. C. N. Diógenes, J. R. de Sousa, I. M. M. de Carvalho, M. L. A. Temperini, A. A. Tanaka, I. S. Moreira, *Dalton Trans.* **2003**, 2231–2236.
[21] H. Liu, H. Yamamoto, J. Wei, D. H. Waldeck, *Langmuir* **2003**, *19*, 2378–2387.
[22] a) T. D. Dolidze, D. E. Khoshtariya, D. H. Waldeck, J. Macyk, R. van Eldik, *J. Phys. Chem. B* **2003**, *107*, 7172–7179; b) D. E. Khoshtariya, T. D. Dolidze, D. Sarauli, R. van Eldik, *Angew. Chem.* **2006**, *118*, 283–287; *Angew. Chem. Int. Ed.* **2006**, *45*, 277–281; c) D. E. Khoshtariya, T. D. Dolidze, S. Seifert, D. Sarauli, G. Lee, R. van Eldik, *Chem. Eur. J.* **2006**, *12*, 7041–7056.
[23] a) M. J. Tarlov, E. F. Bowden, *J. Am. Chem. Soc.* **1991**, *113*, 1847–1849; b) S. Song, R. A. Clark, E. F. Bowden, M. J. Tarlov, *J. Phys. Chem.* **1993**, *97*, 6564–6572.
[24] D. H. Murgida, P. Hildebrandt, *J. Am. Chem. Soc.* **2001**, *123*, 4062–4068.
[25] X. Chen, R. Ferrigno, J. Yang, G. M. Whitesides, *Langmuir* **2002**, *18*, 7009–7015.
[26] a) K. Ataka, J. Heberle, *J. Am. Chem. Soc.* **2003**, *125*, 4986–4987; b) K. Ataka, J. Heberle, *J. Am. Chem. Soc.* **2004**, *126*, 9445–9457.
[27] a) K. Niki, J. R. Sprinkle, E. Margoliash, *Bioelectrochemistry* **2002**, *55*, 37–40; b) K. Niki, W. R. Hardy, M. G. Hill, H. Li, J. R. Sprinkle, E. Margoliash, K. Fujita, R. Tanimura, N. Nakamura, H. Ohno, J. H. Richards, H. B. Gray, *J. Phys. Chem. B* **2003**, *107*, 9947–9949.
[28] J. J. Wei, H. Liu, K. Niki, E. Margoliash, D. H. Waldeck, *J. Phys. Chem. B* **2004**, *108*, 16912–16917.
[29] S. Imabayashi, T. Mita, T. Kakiuchi, *Langmuir* **2005**, *21*, 2474–2479.
[30] M. T. de Groot, T. H. Evers, M. Merkx, M. T. M. Koper, *Langmuir* **2007**, *23*, 729–736.
[31] a) H. Yamamoto, H. Liu, D. H. Waldeck, *Chem. Commun.* **2001**, 1032–1033; b) J. Wei, H. Liu, A. R. Dick, H. Yamamoto, Y. He, D. H. Waldeck, *J. Am. Chem. Soc.* **2002**, *124*, 9591–9599; c) J. Wei, H. Liu, D. E. Khoshtariya, H. Yamamoto, A. Dick, D. H. Waldeck,

Angew. Chem. **2002**, *114*, 4894–4897; *Angew. Chem. Int. Ed.* **2002**, *41*, 4700–4703; d) D. E. Khoshtariya, J. Wei, H. Liu, H. Yue, D. H. Waldeck, *J. Am. Chem. Soc.* **2003**, *125*, 7704–7714; e) D. H. Murgida, P. Hildebrandt, J. Wei, Y.-F. He, H. Liu, D. H. Waldeck, *J. Phys. Chem. B* **2004**, *108*, 2261–2269; f) H. Yue, D. Khoshtariya, D. H. Waldeck, J. Grochol, P. Hildebrandt, D. H. Murgida, *J. Phys. Chem. B* **2006**, *110*, 19906–19913.

[32] J. C. Love, L. A. Estroff, J. K. Kriebel, R. G. Nuzzo, G. M. Whitesides, *Chem. Rev.* **2005**, *105*, 1103–1169.

[33] a) M. Mrksich, J. R. Grunwell, G. M. Whitesides, *J. Am. Chem. Soc.* **1995**, *117*, 12009–12010; b) J. Lahiri, L. Isaacs, J. Tien, G. M. Whitesides, *Anal. Chem.* **1999**, *71*, 777–790; c) J. Lahiri, L. Isaacs, B. Grzybowski, J. D. Carbeck, G. M. Whitesides, *Langmuir* **1999**, *15*, 7186–7198; d) R. G. Chapman, E. Ostuni, L. Yan, G. M. Whitesides, *Langmuir* **2000**, *16*, 6927–6936; e) E. Ostuni, B. A. Grzybowski, M. Mrksich, C. S. Roberts, G. M. Whitesides, *Langmuir* **2003**, *19*, 1861–1872.

[34] I. Takahashi, T. Inomata, Y. Funahashi, T. Ozawa, K. Jitsukawa, H. Masuda, *Chem. Commun.* **2005**, 471–473.

[35] a) K. Bernauer, J.-J. Sauvain, *J. Chem. Soc. Chem. Commun.* **1988**, 353–354; b) K. Bernauer, M. Monzione, P. Schürmann, V. Viette, *Helv. Chim. Acta* **1990**, *73*, 346–352; c) K. Bernauer, P. Jauslin, *Chimia* **1993**, *47*, 218–220; d) K. Bernauer, L. Verardo, *Angew. Chem.* **1996**, *108*, 1823–1825; *Angew. Chem. Int. Ed. Engl.* **1996**, *35*, 1716–1717; e) K. Bernauer, S. Ghizdavu, L. Verardo, *Coord. Chem. Rev.* **1999**, *190–192*, 357–369; f) U. Scholten, A. C. Merchán, K. Bernauer, *J. R. Soc. Interface* **2005**, *2*, 109–112.

[36] a) S. Sakaki, Y. Nishijima, H. Koga, K. Ohkubo, *Inorg. Chem.* **1989**, *28*, 4061–4063; b) S. Sakaki, Y. Nishijima, K. Ohkubo, *J. Chem. Soc. Dalton Trans.* **1991**, 1143–1148.

[37] a) J. T. Ficke, J. R. Pladziewicz, E. C. Sheu, A. G. Lappin, *Inorg. Chem.* **1991**, *30*, 4282–4285; b) J. R. Pladziewicz, S. O. Gullerud, M. A. Accola, *Inorg. Chim. Acta* **1994**, *225*, 151–156.

[38] S. Marx-Tibbon, E. Katz, I. Willner, *J. Am. Chem. Soc.* **1995**, *117*, 9925–9926.

[39] G. Tao, E. Katz, I. Willner, *Chem. Commun.* **1997**, 2073–2074.

[40] a) H. Kumita, N. Asai, T. Sakurai, K. Jitsukawa, T. Ozawa, H. Masuda, H. Einaga, *Inorg. Chem. Commun.* **2000**, *3*, 185–187; b) T. Kato, I. Takahashi, Y. Funahashi, T. Ozawa, H. Masuda, *Adv. Mater. Res.* **2006**, *11–12*, 343–346; c) T. Kato, H. Kumita, I. Takahashi, A. Murakami, K. Yoshimoto, Y. Ikeue, K. Kataoka, S. Suzuki, T. Sakurai, T. Ozawa, K. Jitsukawa, H. Masuda, *Inorg. Chim. Acta* **2007**, *360*, 1555–1567; d) T. Kato, I. Takahashi, H. Kumita, T. Ozawa, Y. Funahashi, K. Jitsukawa, H. Masuda, *Bull. Chem. Soc. Jpn.* **2007**, in press.

[41] a) H. Kumita, K. Jitsukawa, H. Masuda, H. Einaga, *Inorg. Chim. Acta* **1998**, *283*, 160–166; b) H. Kumita, T. Morioka, T. Ozawa, K. Jitsukawa, H. Einaga, H. Masuda, *Bull. Chem. Soc. Jpn.* **2001**, *74*, 1035–1042; c) H. Kumita, T. Kato, K. Jitsukawa, H. Einaga, H. Masuda, *Inorg. Chem.* **2001**, *40*, 3936–3942.

[42] S. Chao, J. L. Robbins, M. S. Wrighton, *J. Am. Chem. Soc.* **1983**, *105*, 181–188.

[43] For example, the surface coverage of (*S*)-**2**–Au immersed for 3 d at 5 °C was 3.5×10^{-11} mol cm^{-2}.

[44] C. A. Widrig, C. Chung, M. D. Porter, *J. Electroanal. Chem.* **1991**, *310*, 335–359.

[45] G. E. Poirier, *Chem. Rev.* **1997**, *97*, 1117–1127.

[46] a) F. G. Chevallier, L. Jiang, T. G. J. Jones, R. G. Compton, *J. Electroanal. Chem.* **2006**, *587*, 254–262; b) F. G. Chevallier, N. Fietkau, J. del Campo, R. Mas, F. X. Muñoz, L. Jiang, T. G. J. Jones, R. G. Compton, *J. Electroanal. Chem.* **2006**, *596*, 25–32.

[47] *Electrochemical Methods, Fundamentals and Applications* (Eds.: A. J. Bard, L. R. Faulkner), 2nd ed., Wiley, New York, **2001**.

[48] I. Takahashi, T. Inomata, Y. Funahashi, T. Ozawa, H. Masuda, *Chem. Lett.* **2006**, 1404–1405.

[49] C. E. D. Chidsey, C. R. Bertozzi, T. M. Putvinski, A. M. Mujsce, *J. Am. Chem. Soc.* **1990**, *112*, 4301–4306.

[50] $E_{pa/2}$ and $E_{pc/2}$ are the anodic and cathodic half-peak potentials, respectively.

[51] In the **3–Au**–$[Ru(NH_3)_6]^{3+}$ system, the anodic and cathodic peak shifts were estimated from the peak potentials at 50 mV s^{-1}.

[52] P. X. Qi, R. A. Beckman, A. J. Wand, *Biochemistry* **1996**, *35*, 12275–12286.

[53] A. M. Berghuis, G. D. Brayer, *J. Mol. Biol.* **1992**, *223*, 959–976.

[54] C. Weber, B. Michel, H. R. Bosshard, *Proc. Natl. Acad. Sci. USA* **1987**, *84*, 6687–6691.

[55] P. Hildebrandt, M. Stockburger, *Biochemistry* **1989**, *28*, 6722–6728.

[56] W. J. Albery, M. J. Eddowes, H. A. O. Hill, A. R. Hillman, *J. Am. Chem. Soc.* **1981**, *103*, 3904–3910.

[57] S. Korman, H. T. Clarke, *J. Biol. Chem.* **1956**, *221*, 113–131.

[58] K. Jitsukawa, T. Morioka, H. Masuda, H. Ogoshi, H. Einaga, *Inorg. Chim. Acta* **1994**, *216*, 249–251.

[59] H. Angerstein-Kozlowska, B. E. Conway, A. Hamelin, L. Stoicoviciu, *J. Electroanal. Chem.* **1987**, *228*, 429–453.

Received: January 30, 2007
Published online: July 6, 2007

